PHYSICAL REVIEW B **78**, 214302 (2008)

Detecting quantum-coherent nanomechanical oscillations using the current-noise spectrum of a double quantum dot

Neill Lambert[1,*] and Franco Nori[1,2]

[1]*Advanced Science Institute, The Institute of Physical and Chemical Research (RIKEN), Saitama 351-0198, Japan*

[2]*Department of Physics, Center for Theoretical Physics, Applied Physics Program, Center for the Study of Complex Systems, The University of Michigan, Ann Arbor, Michigan 48109-1040, USA*

(Received 1 September 2008; revised manuscript received 4 November 2008; published 12 December 2008)

We consider a nanomechanical resonator coupled to a double quantum dot. We demonstrate how the finite-frequency current-noise spectrum through the double quantum dot can be used to distinguish classical and quantum behavior in the nearby nanoelectromechanical resonator. We also show how the full-frequency current-noise spectrum gives important information on the combined double quantum dot-resonator energy spectrum. Finally, we point out regimes where the quantum state of the resonator becomes squeezed and also examine the cross-correlated electron-phonon current noise.

DOI: 10.1103/PhysRevB.78.214302 PACS number(s): 62.25.Jk, 72.70.+m, 73.63.Kv

I. INTRODUCTION

The transduction of mechanical motion of resonators and cantilevers[1–6] has become increasingly important with the observation of motion on the nanometer scale. In particular, when the ground-state energy of the resonant mode of the mechanical system becomes larger than the thermal background temperature, a quantized state involving millions of molecules would materialize. As nanoelectromechanical systems (NEMSs) reach this regime it becomes increasingly feasible and desirable to transduce their motion by coupling it to a quantum degree of freedom, such as spin,[7] charge,[8] or flux. However, the challenge of finding an appropriate measuring apparatus, one whose back action would not destroy the fragile quantum state, has not been overcome, even if such devices could be cooled below the quantum limit.[9,10]

Here we propose using a quantized two-level "mesoscopic transport" degree of freedom or "transport qubit" as a transducer of quanta exchange and identify signatures of quantum-coherent *coupled* phenomena between the mechanical resonator and the transport qubit. If successfully observed, this would validate the existence of a quantized mechanical state. Here we focus on a capacitively coupled double quantum dot realization for the transport qubit. However, our analysis applies to several other possible devices, such as superconducting single-electron transistors (SSETs) (Ref. 9) and suspended double quantum dots,[11] which will be described later.

A. Probing mesoscopic transport

It is important to note that the types of experimental measurement that can be made on mesoscopic transport systems are limited; we can measure the average rate of particles leaving the system (current), the correlation between these currents at long times (the zero-frequency noise), and the full Fourier transform of these correlations (full-frequency noise). Over the last few years, the zero-frequency noise has been used with great success to experimentally verify coherent quantum behavior (see, e.g., Ref. 12) and may in the future serve as an entanglement measure[13] and perhaps even aid in realizing a solid-state test of Bell's inequalities.[14] The *full-frequency noise spectrum*, often more difficult to measure in practice, is appealing because it contains information about the full dynamics of the system; it reveals both coherent dynamics stemming from the system Hamiltonian H and incoherent dynamics from the environment. This makes it a powerful tool for probing solid-state quantum systems.

B. Summary of our results

Our main result here is that we show how the coupled quantum-coherent behavior, e.g., Rabi oscillations, and the low-energy part of the coupled double quantum dot-resonator spectrum can be observed as resonances in the *full-frequency current-noise* spectrum. We also analyze the effects of temperature and decoherence on this signal and show how the transition to the classical regime can be monitored using our approach.

We now proceed as follows: we first define a general model for a transport "qubit" coupled to the quantized fundamental mechanical mode of a nanoelectromechanical resonator. This is a well-studied model in various forms and has been used to illustrate, e.g., boson steering and micromaser effects.[8,15,16] Following this, we explain why *current-noise measurements* can contain signatures of *quantum-coherent* behavior. We illustrate this with results from our master-equation model for two different parameter regimes. We also identify signatures of quantum state squeezing[17] of the resonator, and we calculate the correlation between tunneling events in the transport qubit and phonons leaving the mechanical resonator. Finally, we discuss other possible experimental realizations, such as suspended double quantum dots,[11,15,18] spin states coupled to a magnetized resonator,[7] and capacitively coupled superconducting single-electron transistors.[9]

II. MODEL: TRANSPORT QUBIT COUPLED TO A MECHANICAL MODE

The basic Hamiltonian for a transport qubit coupled to a quantized mechanical resonator is as follows:

$$H = \epsilon\sigma_z + \Delta\sigma_x + g\sigma_z(a + a^\dagger) + \omega_b a^\dagger a. \quad (1)$$

Here ω_b is the fundamental frequency of the resonator, ϵ is the energy gap, or splitting, of the transport qubit states, and Δ is the coherent tunneling rate between the two qubit states. The bosonic operators $a, a^\dagger$ destroy and create excitations in the resonator. The quasispin basis describes the two possible states in our transport qubit, and we assume that the transport process enters and leaves through the eigenstates of σ_z. For example, for our case of a double quantum dot in the Coulomb blockade regime (as shown in Fig. 1), $\sigma_z = |L\rangle\langle L| - |R\rangle\langle R|$, where L and R represent an excess electron ($N+1$ total electrons) in the left or right dot, and the state $|0\rangle$ represents the empty state (N total electrons). Note that the excess electron in the double dot is well separated in energy from the other electrons due to Coulomb blockade. Alternatively, the superconducting single-electron transistor can be defined by $\sigma_z = |2\rangle\langle 2| - |0\rangle\langle 0|$, representing the superposition of charge states on the island. Even though superconducting single-electron transistors are three-terminal devices, in certain regimes the model is equivalent to a double quantum dot[19] (see below). The spin-blockade case would involve a direct coupling, via the magnetization of the resonator,[7] to the electron spin $\sigma_z = |\uparrow\rangle\langle\uparrow| - |\downarrow\rangle\langle\downarrow|$. Hereafter we retain the double quantum dot basis, $\{|L\rangle, |R\rangle\}$.

A. Master equation

Transport, in all these cases, is in nonequilibrium (left to right), with a large bias applied to the device, and the current measurement monitors the electrons or particles leaving the device into the right lead or reservoir (here we neglect displacement-current contributions). The full equation of motion (master equation) for this system is described by a superoperator Liouvillian L that defines the transport of particles through the qubit (under the Born-Markovian approximation), bath damping, and temperature terms for the resonator,

$$\frac{d}{dt}\rho(t) = L[\rho(t)] = -i[H, \rho(t)] + L_0[\rho(t)],$$

$$\begin{aligned} L_0[\rho(t)] = &-\frac{\Gamma_L}{2}[s_L s_L^\dagger \rho(t) - 2s_L^\dagger \rho(t) s_L + \rho(t) s_L s_L^\dagger] \\ &-\frac{\Gamma_R}{2}[s_R^\dagger s_R \rho(t) - 2s_R \rho(t) s_R^\dagger + \rho(t) s_R^\dagger s_R] \\ &+\frac{\gamma_b}{2}[-a^\dagger a\rho + 2a\rho a^\dagger - \rho a^\dagger a] \\ &+\bar{n}\gamma_b[-a^\dagger a\rho + a\rho a^\dagger + a^\dagger \rho a - \rho a^\dagger a], \end{aligned} \quad (2)$$

where

$$s_L = |0\rangle\langle L|, \quad s_L^\dagger = |L\rangle\langle 0|, \quad (3)$$

$$s_R = |0\rangle\langle R|, \quad s_R^\dagger = |R\rangle\langle 0|, \quad (4)$$

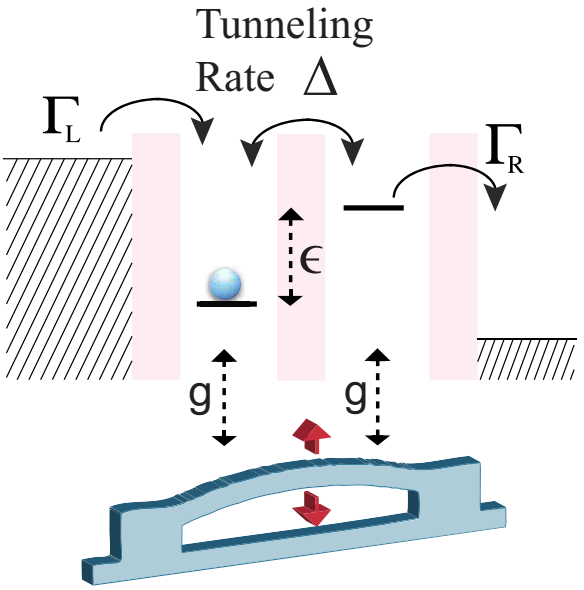

FIG. 1. (Color online) Schematic diagram of a double quantum dot transport qubit (pink) coupled to a mechanical resonator (in blue). We assume a capacitive coupling g between the position of the resonator and the electron charge state of the electron in the dot. The double quantum dot is attached to two electron reservoirs in the Coulomb blockade regime, with tunneling rates Γ_L and Γ_R. There is a coherent tunneling rate Δ between the two charge states and a tunable energy gap ϵ. We assume that the mechanical resonator is already cooled near the quantum limit (Refs. 9 and 10). The parameter g is the coupling strength between the double quantum dot and the mechanical resonator, whose fundamental frequency is ω_b. In the schematic diagram, the placement of the components is purely illustrative. Our model is also applicable to circuit-QED systems, where coherent energy exchange between a resonator and a two-level system has recently been observed (see, e.g., Ref. 21).

$$\bar{n} = e^{-\hbar\omega_b/kT}/(1 - e^{-\hbar\omega_b/kT}), \quad (5)$$

Γ_L and Γ_R are the left or right tunneling rates, γ_b is the decay rate of vibrational quanta into the resonator thermal bath, and T is the temperature of the resonator thermal bath (hereafter we set $k = \hbar = 1$). $\rho(t)$ is the density matrix describing the state of the resonator and the qubit.

B. Current-noise power

We derive the counting statistics of Eq. (2) using a generating-function approach (Appendix). Using these equations we can calculate the current-noise power,[20]

$$S(\omega)_{i,j} \equiv \int_{-\infty}^{\infty} d\tau e^{i\omega\tau}[\langle \delta I_i(t+\tau), \delta I_j(t)\rangle]_{t\to\infty}, \quad (6)$$

where $\delta I_i(t)$ are the current fluctuations and $t \to \infty$ implies that the fluctuations are around the steady-state expectation values. This formalism describes the following:

(i) particle transport through our effective qubit ($i=j=e$, electron or particle current),

(ii) statistics of bunching "vibrational phonons" lost to the background thermal bath of the resonator ($i=j=b$, where I_b is an effective "bosonic" current), and

(iii) correlations between electron and phonon events ($i \neq j$, $i=e$, $j=b$).

The electron current is defined by the operator

$$\hat{I}_e = \Gamma_R s_R \rho(t) s_R^\dagger. \tag{7}$$

Similarly, the vibrational phonon current is defined by the operator

$$\hat{I}_b = \gamma_b a \rho(t) a^\dagger. \tag{8}$$

Even though such "phonon statistics" are typically not experimentally accessible, we include them here because of the connections of our model to circuit-QED systems,[21–25] where the *photon* statistics can be probed with incident microwave fields and the state of the pseudospin (qubit) by suitable detectors. Such a system would also be suitable for observing the cross-correlation measurements we will present later. Also, it is interesting to point out that in some sense the vibrational mode of the resonator itself can be thought of as an "acoustic phonon" with low frequency and long wavelength. Thus in this paper, for brevity we often refer to the "vibrational quanta of the fundamental mode of the resonator" as phonons.

III. POLES IN THE CURRENT-NOISE FREQUENCY SPECTRUM

To understand why the current-noise spectrum contains direct signatures of coherent quantum behavior, we must consider its dependence on the superoperator L. As discussed by Emary *et al.*[26] and Flindt *et al.*[27] the eigenvalues, α_k, of the superoperator L [e.g., Eq. (2)] consist of imaginary "coherent" quantum-mechanical level-splitting terms, originating from H, and of real "incoherent" terms, originating from background thermal baths and nonequilibrium tunneling events. This can be seen by expanding the density matrix ρ of the coupled system across the eigenstates of H, $\rho = \Sigma_{i,j} c_{i,j} |i\rangle\langle j|$, then the Liouvillian L acts as

$$L[\rho] = -iH\rho + i\rho H + L_0[\rho] = -i(\lambda_i - \lambda_j)\rho + L_0[\rho]. \tag{9}$$

As mentioned above, since all the operators in L_0 are real, the eigenvalues of L will consist of imaginary terms due to energy-level splitting,

$$\delta E = (\lambda_i - \lambda_j), \tag{10}$$

and real terms from operators in L_0.

In certain conditions,[26] the current-noise power can be expanded in terms of eigenvalues α_k of L and the coefficients c_k of the matrix $(V^{-1}\hat{I}_e V)_{kk}$, where $\hat{I}_e$ is the current operator discussed earlier and V are the eigenvectors of L, so that

$$S(\omega) = 1 - 2\sum_{k=1}^{N_v} \frac{c_k \alpha_k}{\omega^2 + \alpha_k^2}. \tag{11}$$

Here, N_v is the dimension of the superoperator L. If the incoherent terms, those outside the commutator in the Liouvillian L [e.g., in Eq. (2)], are much bigger than the coherent energy-level splitting δE (e.g., $\Gamma_{L,R}, \gamma \gg \delta E$), then the eigenvalues of the Liouvillian are real, and the quantum noise is a

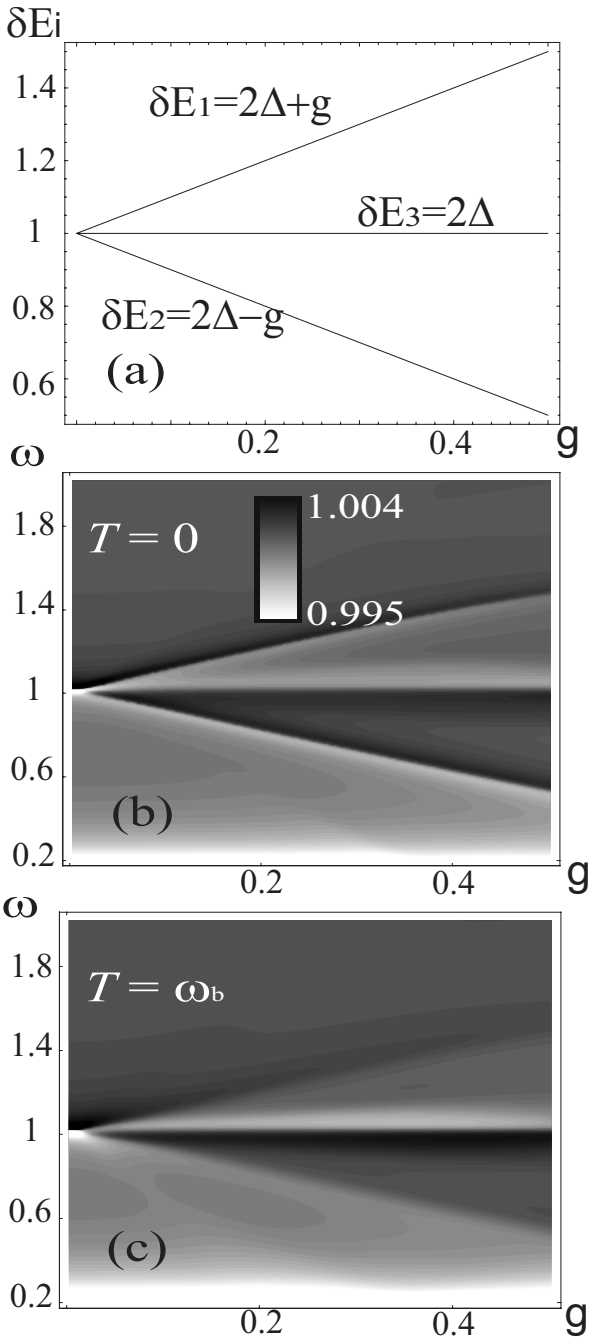

FIG. 2. (a) shows the three important energy gaps (δE_i, $i=1,2,3$) in the low-level energy spectrum of the Jaynes-Cummings Hamiltonian (see text). The parameter g is the coupling between the electron and the resonator. (b) and (c) show, as contour plots, how these gaps can be observed in the current-noise frequency spectrum $S(\omega)_{e,e}/2eI_e$ for $\omega_b=1$, $\Gamma_L=\Gamma_R=0.01$, $\Delta=0.5$, $\gamma_b=0.05$, and $T=0, \omega_b$. The energy gaps shown in (a) are clearly visible as three resonances in (b) and (c). The horizontal line corresponds to the physical process of an electron tunneling without exchanging quanta with the resonator. The top and bottom resonant lines are proportional to the coupling g and thus represent the physical process of the electron coherently emitting a phonon into the resonator. As the temperature is increased, the visibility of the two "Rabi peaks," which are signatures of coherent quantum behavior of the resonator, decreases.

slowly varying function of frequency. If, however, the coherent terms in Eq. (2) dominate, then there exist poles in the current-noise spectrum around the absolute value of the energy-level splitting,[26]

$$\omega = |\delta E + i\Gamma + O(\Gamma/\delta E)|, \tag{12}$$

giving rise to the resonant features we seek.

IV. OBSERVATION OF QUANTUM COHERENCE

To illustrate how to observe quantum signatures, we now investigate the above model [Eq. (2)] in two regimes: (1) an effective Jaynes-Cummings regime (when the level-splitting matches the resonator frequency $2\Delta=\omega_b$) and (2) an off-resonance regime (where $2\Delta \neq \omega_b$). Later on we will look at the zero-frequency noise and make a comparison to a recent experiment which measured the zero-frequency noise of a double quantum dot in contact with a many-mode phonon bath.

Hereafter, all results are calculated using the master equation and noise formalism described above, with a bosonic cutoff appropriate for the parameter regimes being discussed. We also discuss, where appropriate, the dynamics of an effective pure state to understand how the energy spectrum of H contributes to the spectral structure of the noise.

A. First regime: Effective Jaynes-Cummings Hamiltonian

An effective Jaynes-Cummings Hamiltonian can be realized if we set $\epsilon=0$ and $2\Delta=\omega_b$. Then,

$$H = \Delta\sigma_x + g\sigma_z(a+a^\dagger) + \omega_b a^\dagger a. \tag{13}$$

Large Δ implies[18] that there is a strong overlap between the particle wave functions in the two states, which may introduce extra coupling terms with the resonator. However, for simplicity, we assume that they are negligible.

First, we write the diagonal energy term for the qubit (σ_z) in the off-diagonal basis (σ_x) by substituting raising and lowering operators in that basis,

$$\sigma_x^+ = \frac{1}{2}(\sigma_z - i\sigma_y), \quad \sigma_x^- = \frac{1}{2}(\sigma_z + i\sigma_y). \tag{14}$$

Then performing the rotating-wave approximation in this basis, by dropping counter-rotating terms, we obtain

$$\begin{aligned} H_{\mathrm{JC}} &\approx g(\sigma_x^+ a + \sigma_x^- a^\dagger) + \omega_b a^\dagger a + \Delta\sigma_x \\ &= g\left[\frac{1}{2}(\sigma_z - i\sigma_y)a \right. \\ &\quad \left. + \frac{1}{2}(\sigma_z + i\sigma_y)a^\dagger\right] + \omega_b a^\dagger a + \Delta\sigma_x. \end{aligned} \tag{15}$$

This has the spectrum of an infinite number of noninteracting multiplets with eigenstates,

$$|\pm\rangle_n = \frac{1}{\sqrt{2}}(|n,1_x\rangle \pm |n+1,0_x\rangle, \tag{16}$$

where $|n\rangle$ is the number state of the mechanical resonator and $|0\rangle_x$ and $|1\rangle_x$ are the eigenstates of σ_x (i.e., the bonding and antibonding states within the double quantum dot).

If we consider the zero-temperature limit and a strong damping of the bath, then only the lowest number states of the mode $n=0,1$ strongly contribute to the transport processes (this case is well into the quantum regime and the ideal situation). This regime is feasible if the effective temperature of the resonator is below $\hbar\omega_b$. In this case, if $\Gamma_L \approx \gamma_b$ then the initial state of each "round" of transport would be

$$|\psi(t=0)\rangle = |0,L\rangle = \frac{1}{\sqrt{2}}(|0,0_x\rangle + |0,1_x\rangle. \tag{17}$$

The second component $|0,1_x\rangle$ couples to the $n=0$ and $n=1$ states of the mechanical resonator via the $|\pm\rangle_{n=0}$ eigenstates of H_{JC}. The first component, $|0,0_x\rangle$, acts as an "interaction free" transport route because it is the ground state of H_{JC}. The component $|0,0_x\rangle$ has a unique "ground-state energy" $E_0=-\Delta$, while the two $|\pm\rangle_{n=0}$ eigenstates of H_{JC} have energies

$$E_\pm = \omega_b/2 \pm \sqrt{\Omega^2 + 4g^2}/2, \tag{18}$$

where

$$\Omega = \omega_b - 2\Delta. \tag{19}$$

Our numerical simulations in Figs. 2 and 3 show clearly how the energy-level *splittings* δE_i $(i=1,2,3)$ form *resonances* in the noise frequency spectrum. In particular, because $\Omega=0$ here,

$$\delta E_{1/2} = E_\pm - E_0 = 2\Delta \pm g \tag{20}$$

are the upper and lower resonance "branches" in Figs. 2 and 3, caused by the coherent coupling between the double quantum dot and the mechanical resonator, and $\delta E_3=2\Delta$ is the central resonance because of coherent internal oscillations within the dot alone. This occurs because of the $|0,0_x\rangle$ ground state of H_{JC}, described above, which only evolves in time with a phase factor $E_0=-\Delta$.

As we increase the temperature of the mechanical resonator thermal bath, the upper and lower resonance branches gradually disappear and the central resonance, determined by $\omega=2\Delta$, dominates. Increasing the temperature of the "bath" means that the mechanical resonator would be in a thermal mixture of number states; thus for the electron, more transport channels become available. This is more clearly apparent in the magnitude of the noise shown in Fig. 3, illustrating that by *monitoring the peaks* in the current-noise transport $S_{e,e}(\omega)$ one can, in principle, *distinguish classical and quantum behavior*. However, the observation of near zero-temperature oscillations is not always proof of quantum behavior[5,28–32] as they can also be described by a classical model of coupled linear oscillators. For example, in our current-noise formulation "false signatures" from interactions of the qubit with nearby classical oscillators may appear in the spectrum and be mistaken for quantum Rabi behavior. We will discuss this further in Sec. IV B.

One can understand the transition to the high-temperature case by assuming the initial state to be

$$|\psi(t=0)\rangle = \left(\sum_n C_n|n\rangle\right) \otimes \frac{1}{\sqrt{2}}(|0_x\rangle + |1_x\rangle), \tag{21}$$

which connects each multiplet in the spectrum of the Jaynes-Cummings Hamiltonian with its two nearest energy levels. The subspace of the Hamiltonian connecting $|n-1,1_x\rangle$, $|n,0_x\rangle$ $|n,1_x\rangle$, and $|n+1,0_x\rangle$ is (where the basis here is for σ_x diagonal)

$$H_{n-1,n,n+1} = \begin{pmatrix} (n-1)\omega_b + \Delta & g\sqrt{n} & 0 & 0 \\ g\sqrt{n} & n\omega_b - \Delta & 0 & 0 \\ 0 & 0 & n\omega_b + \Delta & g\sqrt{n+1} \\ 0 & 0 & g\sqrt{n+1} & (n+1)\omega - \Delta \end{pmatrix}. \tag{22}$$

Then, we easily see that the probability that the left dot is occupied [corresponding to the probability of the superposition of bonding and antibonding states $\frac{1}{\sqrt{2}}(|0_x\rangle + |1_x\rangle)$] is given by

$$P_L(t) = \sum_{n=0}^{\infty} \left\{ C_n \cos\left[\frac{-g(\sqrt{n+1} - \sqrt{n})t - 2t\Delta}{2} \right] \right\}^2. \tag{23}$$

Considering both an equal superposition, $C_n = 1/\sqrt{N}$ [but with cutoff of the sum in $P_L(t)$ at a given N], and a coherent-state distribution, $C_n(z) = z^n e^{-z}/n!$, we observe that the oscillations in the probability $P_L(t)$ collapse over time, until only small oscillations with period Δ around $P_L = 0.5$ remain. This is because the noncommensurate Rabi frequencies in Eq. (23) interfere *destructively*. For a small number of number states N or a small coherent-state distribution z, there is some revival in $P_L(t)$, but as N increases the number of revivals fall. This is also true if the initial state is a separable density matrix with the resonator state in a thermal Boltzman distribution, as is the case for high temperatures.

B. Second regime: Off-resonant interaction

In Sec. IV A we showed that on resonance, $2\Delta = \omega_b$, the lowest part of the energy spectrum of the coupled system was visible in the current noise. We can now verify that these resonances really stem from the low-energy spectrum of the Jaynes-Cummings Hamiltonian and indicate coherent *quantum* dynamics by inspecting the *off-resonant* regime, $2\Delta \neq \omega_b$, where the energy levels have a hyperbolic behavior. In terms of the double-dot realization, we point out that assuming a small Δ implies a tight confinement of the electron within each dot.

Observing Fig. 4(a), we can see upper and lower resonance branches, but in this case ($2\Delta \neq \omega_b$) they have the typical hyperbolic tails of an avoided level crossing. In addition, Fig. 4(b) shows that, as the coupling to the mechanical resonator g is increased, the gap in the level crossing increases. Once more we are successfully observing the low-energy spectrum of the Hamiltonian in the power spectrum of the current noise. For example, the upper and lower branches are simply given by the lowest eigenvalues of the Jaynes-Cummings Hamiltonian,

$$\delta E_{1,2} = |\omega_b/2 \pm \sqrt{\Omega^2 + 4g^2}/2 + \Delta|.$$

Furthermore, we note that there is an energy gap which halts the electron current in the limit when $\epsilon = 0$ and when the coherent tunneling within the dots is small relative to the coupling to the mode, $\Delta \ll g$. This occurs because the tunneling of an electron requires an energy loss proportional to the displacement of the mode and because the rotating-wave approximation is no longer valid. For transport to occur, the electron must tunnel from the left to the right state, which is now shifted in (relative) energy by $2g(a+a^\dagger)$. This becomes more and more difficult as the coupling g is increased, resulting in a "current blockade" effect.

Finally, as discussed in Sec. IV A, we point out that oscillations alone may not provide sufficient proof of quantum behavior. Recent circuit-QED experiments[28,29] have focused on the idea of observing the square-root dependence of the energy of the Jaynes-Cummings system on the photon occupation number n, which is sufficiently distinct from the behavior seen in classical models. However, the preparation of arbitrary Fock states in a nanomechanical resonator is not readily realizable at this point in time.

C. Zero frequency noise: Comparing the single and many-mode cases

In Secs. IV A and IV B we showed how the low-energy levels of a Jaynes-Cummings Hamiltonian can be seen in the *full-frequency* current-noise spectrum. However, most recent experiments have focused on the *zero-frequency* noise. For example, Kieszlich *et al.*[12] showed, by comparing experiment and theory, that coherent oscillations in a double quantum dot produced *super-Poissonian* $[S(0)_{e,e}/2eI_e > 1]$ signatures in the zero-frequency noise, while incoherent transitions (sequential tunneling induced by increasing the temperature of the phonon bath) produce *sub-Poissonian* noise $[S(0)_{e,e}/2eI_e < 1]$.

Mimicking their parameter regime, i.e., considering their device as coupled to a resonator (or phonon cavity), now we also look at the zero-frequency noise (as a function of double

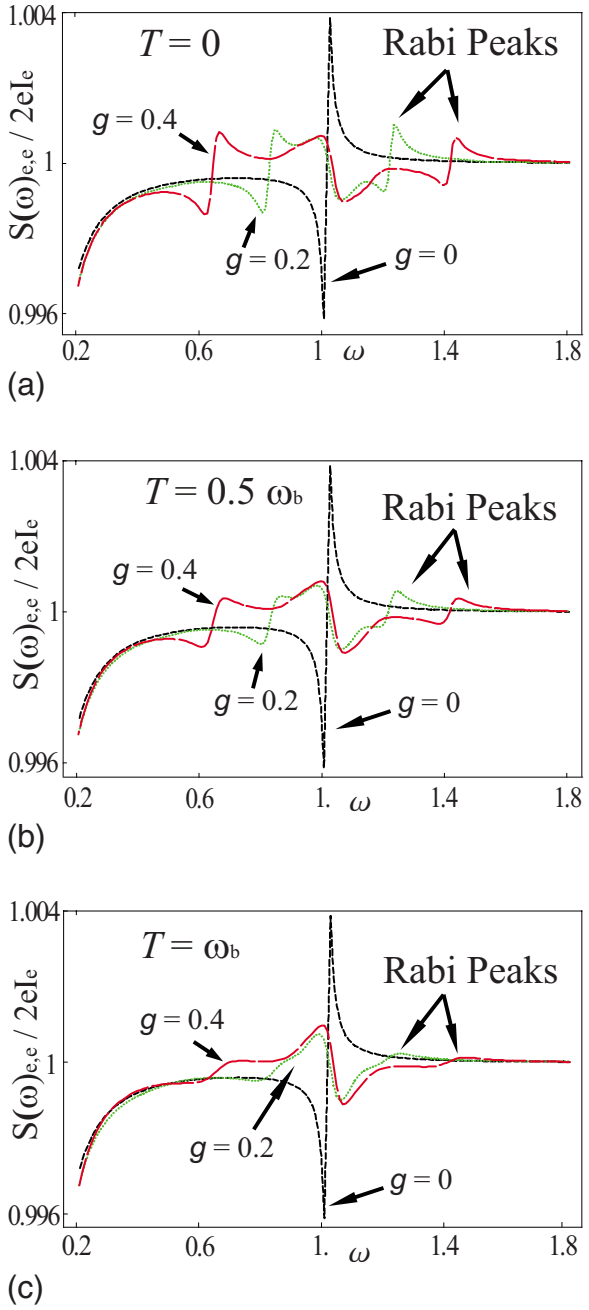

FIG. 3. (Color online) Normalized current-noise frequency spectrum, $S(\omega)_{e,e}/2eI_e$, versus ω for $\omega_b=1$, $\Gamma_L=\Gamma_R=0.01$, $\Delta=0.5$, $\gamma_b=0.05$, and $T=0$, $0.5\omega_b$, ω_b [(a)–(c), respectively] and a selection of electron-resonator coupling strengths g; black, green, and red are $g=0,0.2,0.4$, respectively. The resonances are marked by arrows. As the temperature is increased, the system enters the classical regime and the two Rabi peaks decrease and become hard to distinguish.

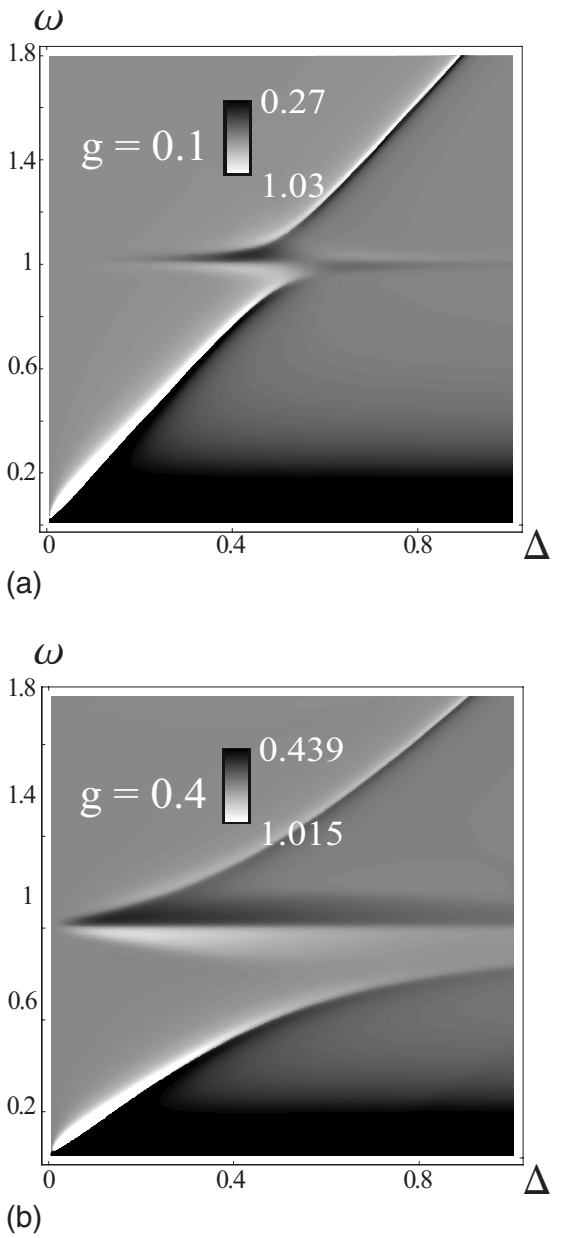

FIG. 4. Current-noise frequency-spectrum, $S(\omega)_{e,e}/2eI_e$, versus both the tunneling rate Δ and frequency ω for (a) $g=0.1$ and (b) $g=0.4$. In both cases $\omega_b=1$, $\Gamma_L=\Gamma_R=0.01$, $\gamma_b=0.05$, $\epsilon=0$, and $T=0$. This was obtained numerically by solving the master equation in Eq. (3). As Δ approaches $\omega_b/2=0.5$ we see the three resonance points previously shown in Fig. 3. Increasing g increases the gap between the resonant peaks. The hyperbolic behavior comes from the well-known Jaynes-Cummings eigenvalue spectrum, as recently observed experimentally in a similar system (e.g., Refs. 21, 28, and 29).

quantum dot level detuning ϵ). We observe similar signatures to theirs in the noise spectrum but with a more complicated structure. We also observe, in Fig. 5(a), that increasing the temperature of the *single-mode* resonator decreases the zero-frequency current noise, eventually resulting in sub-Poissonian behavior.

Similarly, increasing the bare coupling strength g to the single-mode resonator has a drastic effect. As Fig. 5(b) shows, the noise profile quickly becomes sub-Poissonian, developing another peak structure around $\epsilon=1$. Interestingly, the $\epsilon=0$ point, where we earlier probed for coherent signatures, remains around $S(0)_{e,e}/2eI_e=1$, indicating that coherent transport is still occurring.

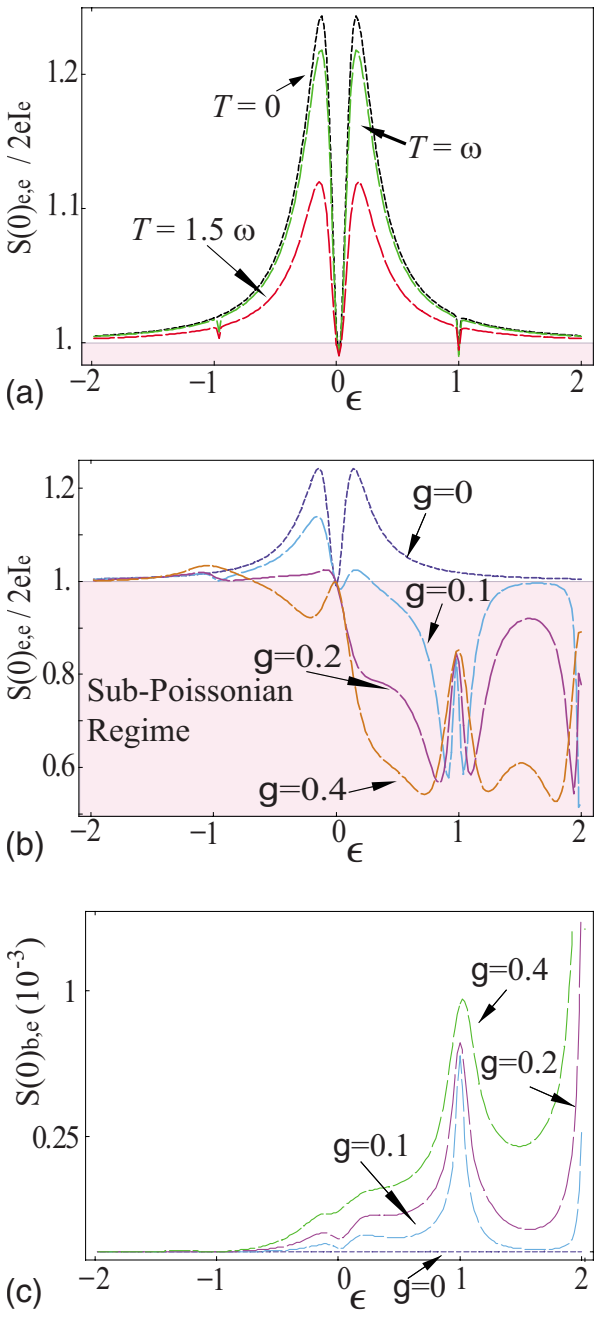

FIG. 5. (Color online) (a) Current-noise frequency-spectrum $S(0)_{e,e}/2eI_e$ versus ϵ for $\omega=1$, $\Gamma_L=0.1$, $\Gamma_R=0.001$, $\Delta=0.1$, $\gamma_b=0.01$, and $g=0.0008$, increasing T from 0 to 2 in steps of 0.5. Increasing the temperature reduces the super-Poissonian character of the current noise. (b) $S(0)_{e,e}/2eI_e$ for $\omega=1$, $\Gamma_L=0.1$, $\Gamma_R=0.001$, $\Delta=0.1$, $\gamma_b=0.01$, and $T=0$ for g from 0 to 0.4 in steps of 0.1 (besides $g=0.3$, which has been omitted for figure clarity). For strong coupling we see that the current noise becomes almost entirely sub-Poissonian (as indicated by the shaded pink region). (c) The cross correlation $S(0)_{e,b}$ against ϵ for the same parameters as (b). Recall that $S(0)_{e,b}$ is defined as the correlation between the electron and phonon currents. For $g=0$ and for negative ϵ there is zero correlation between phonon and electron tunneling, as expected.

Figure 5(c) illustrates the (non-normalized) cross-correlated noise, i.e., the correlation between electron-tunneling events and phonons leaving the mechanical resonator into a heat bath (with rate γ). As expected, there is no correlation between tunneling events when the systems are uncoupled. Furthermore, the correlated noise is large when $\epsilon=k\omega_b$, where k is an integer. While the correlated noise grows for larger k, the current itself becomes smaller.[15] This is simply because as ϵ increases, the current can only flow through phonon-assisted tunneling, which happens at integer numbers of the phonon frequency.

V. SQUEEZING THE QUANTUM STATE OF THE RESONATOR

We have shown that the electron current noise, $S_{e,e}(\omega)$, serves as a detector of coherent interactions between the double quantum dot and the single mode of the mechanical resonator. Already this is a significant step as $S_{e,e}(\omega)$ serves as a tool for experimental observation. However, we can proceed a step further and briefly consider the statistics of the phonons in the mechanical resonator. In such a mechanical system, these quantities are difficult, if not impossible, to access. However, it is informative to understand how the phonon statistics of the resonator change as we increase the temperature and leave the quantum regime.

A. Squeezing signatures

In the proposal by Rodrigues *et al.*[8] they showed that the resonator can exhibit properties akin to a micromaser due to the nonlinear coupling to an SSET. In their case, the qubit is represented by a superposition of island charge states $\sigma_z=|2\rangle\langle 2|-|0\rangle\langle 0|$. However, they focused on the regime where $\omega_b/\Gamma=1$, observing that this is where the interaction between the resonator and SSET is maximized. In the results, we assume that the quantum dots and leads are weakly coupled, $\omega_b/\Gamma\gg 1$, as shown in Secs. I–IV. Furthermore, we assume that the resonator is strongly damped (e.g., via cooling by another SSET or by the double quantum dot itself[10,33]), so that only the few lowest bosonic levels are excited.

However, even for our "slow" regime, we see sub-Poissonian signatures in the *boson emission* noise spectrum emitted into its nearby heat bath $S_{b,b}(0)/2I_b$ as well as in the Fano factor F_Q of the number-state occupation n of the resonator,[34–37]

$$F_Q=\frac{\langle n^2\rangle-\langle n\rangle^2}{\langle n\rangle}, \tag{24}$$

as shown in Figs. 6(a) and 6(b). Both "measures" identify similar regions of squeezing, though there is a conceptual difference between the squeezing of the phonons emitted (dynamically) into the heat bath and a direct measurement of the static steady-state phonon occupation number. Furthermore, we see that as the temperature is increased, both quantities increase nonlinearly in magnitude.

In addition, we consider the correlated electron-phonon noise. We naively expect that stronger correlations will occur in the quantum regime. Figure 6(c) verifies this and shows

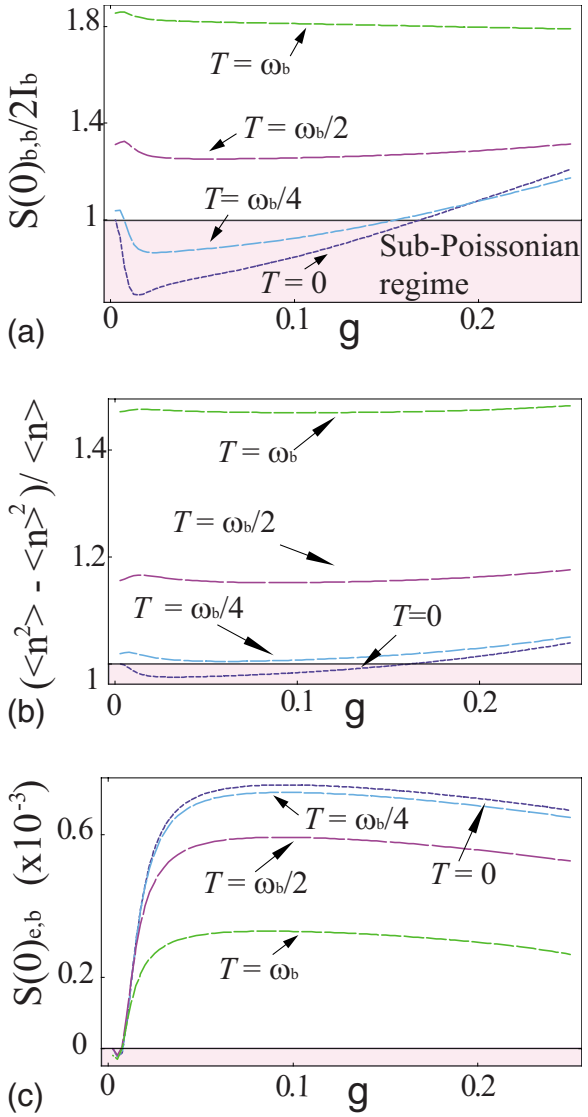

FIG. 6. (Color online) (a) Bosonic current-noise frequency spectrum, $S_{b,b}(\omega)/2I_b$, versus g for $\omega_b=1$, $\Gamma_L=\Gamma_R=0.01$, $\Delta=0.5$, $\gamma_b=0.05$, $\epsilon=0.0$, and a range of temperatures. The pink regions [also denoted by sub-Poissonian regime in (a)] indicate the regimes where quantum state squeezing occurs for low-temperature and intermediate couplings. (b) shows the number-state Fano factor $(\langle n^2\rangle-\langle n\rangle^2)/\langle n\rangle$ of the bosonic system. The zero-temperature case closely corresponds to the "phonon current noise" in (a). (c) shows the electron-phonon correlated noise $S_{e,b}(0)$ versus g. Interestingly, *increasing* the temperature *decreases* the *correlated* noise. Moreover, and as expected, the zero coupling point ($g=0$) remains around $S(0)_{e,b}=0$ for all values of temperature. Also, in a very small regime of weak coupling ($g\to 0$), $S(0)_{e,b}$ can be negative.

that a maximum in the correlated noise occurs around $g=0.1$, and an increase in temperature reduces the overall magnitude. This is an indication, continuing from previous suggestive results,[13] that the quantum noise correlation between two open systems could serve as a measure of entanglement, though a direct correspondence has yet to be identified.

B. Quadrature versus number-state squeezing

The squeezing in Fig. 6 is *number-state squeezing*, and a sub-Poissonian variance in n (F_Q) implies antibunching of the phonon statistics.[38] This is only one of several types of squeezing. For example, in quantum optics, generalized quadrature squeezing is often investigated. Typically the axis of squeezing might not been known, so a homodyne measurement of the occupation statistics must be performed. A homodyne measurement,[39] using a local oscillator to introduce a relative phase, reveals the variance of any desired quadrature. Thus, in principle, it is possible to measure the normal ordered squeezing via

$$\langle:(\Delta Q)^2:\rangle = \langle:Q^2:\rangle - \langle Q\rangle^2, \tag{25}$$

where Q is the quadrature defined by a desired angle ϕ, so that

$$Q = ae^{-i\phi} + a^\dagger e^{i\phi}. \tag{26}$$

Squeezing of the quadrature is implied when

$$\langle:(\Delta Q)^2:\rangle < 0 \tag{27}$$

for some given ϕ because of the normal ordering. Again, in a nanomechanical system such a measurement is not feasible but has been proposed in transmission line resonators.[40] It is trivial to see

$$\langle:(\Delta Q)^2:\rangle = \langle a^{\dagger 2}\rangle e^{2i\phi} + \langle a^2\rangle e^{-2i\phi} + 2\langle a^\dagger a\rangle - \langle a^\dagger\rangle^2 e^{2i\phi} + \langle a\rangle^2 e^{-2i\phi} + 2\langle a\rangle\langle a^\dagger\rangle. \tag{28}$$

However, for our model and parameter space, we were not able to observe any instance of quadrature squeezing. In Secs. I–IV we discussed how strong contributions to the steady-state solution of the master equation arise from the low-level Jaynes-Cummings eigenstates. Our results illustrate that, in our system, these states only produce number-state squeezing in the resonator mode but not quadrature squeezing.[38]

VI. REALIZATIONS

As mentioned before, our model can correspond to charge states in a double quantum dot in a capacitively coupled or suspended geometry. For the suspended geometry,[11,15] it has been shown that there is a direct coupling between the electron wave function and a single phonon mode because of van-Hove singularities in the density of states. However such experiments have not yet been performed in the energy regime of the fundamental *vibrational* mode of a mechanical resonator. Also, our model is related to that of a superconducting single-electron transistor (SSET) capacitively coupled to the resonator.[8,9,19] Typically there are some differences in the transport properties as an SSET is a three-terminal device, and the SSET drives the resonator into complex types of limit-cycle behavior.[8,41]

A. Energy scales

To check the feasibility of our results we need to verify the appropriate energy scales in real systems. We assume that

our state-of-the-art resonator has a fundamental frequency of $\omega_b = 1$ GHz. The corresponding "resonant" bias, $\epsilon = \hbar\omega$, is approximately 4 μeV. We assume we are near the quantum limit, i.e., $kT \approx \hbar\omega_b$, $T \approx 50$ mK. Normal capacitive coupling strengths for an SSET are 100 MHz, corresponding to $g = \omega/10$. In Fig. 2 we saw signatures of quantum-coherent oscillations for this range of coupling strengths. The same range ($g \sim \omega/10$) is feasible for the coupling between a double quantum dot and the resonator (with capacitive coupling[10]). The achievable coupling strengths for suspended geometries are not precisely known now, but because of van-Hove singularities in the density of states one can expect large effective coupling strengths.[11,15] Finally, the interstate tunneling, denoted by Δ in our discussion, is typically tunable for double quantum dots. Thus a range of $\Delta \sim 1$ to 10 μeV is feasible.

B. Magnetized resonator interacting with electron spins

A recent proposal[7] focused on a magnetized resonator which interacts with one of the two electron spins in a spin-blockaded double quantum dot system. In this case, the current is used to measure the spin state because, if the two spins are parallel, current cannot flow. An oscillating magnetic field, from the magnetized resonator, couples to one of the spin states, and thus this spin plays the role of a transport qubit in our earlier language. The question of cooling such a magnetized resonator and then coupling it to a nearby electron spin via its quantized motion and henceforth the quantized magnetic-field motion has not been addressed. In that case, the Hamiltonian of the spin and the resonator is

$$H_Q = -\frac{\Sigma\sigma_z}{2} + \hbar\omega_b a^\dagger a + C\sqrt{\frac{\hbar}{2m_{\text{eff}}\omega_b}}(a + a^\dagger)\sigma_x, \quad (29)$$

where $C = 0.16$ mT/nm. This [Eq. (29)] differs from the Hamiltonians in Eqs. (13) and (15) and that in Eq. (29) is diagonal in the qubit energy basis. The ground-state motion of a 1 GHz resonator is 2×10^{-14} m, which, using the parameters from Ref. 7, would generate a field of just 3.2×10^{-6} mT and a Rabi frequency of about 100 Hz, which is negligible in comparison to nuclear hyperfine and spin-orbit effects. Optimizing device design can increase this Rabi frequency considerably. For example, a larger magnetization could be achieved by using a dysprosium (Dy) micromagnet instead of cobalt (Co) (giving a factor of about 2). Similarly, a larger micromagnet thickness could also contribute a factor of about 2 to the field felt by the electron spin. Decreasing the distance between the dot and resonator could contribute up to a factor of 10, and using a slower frequency resonator, for a larger ground-state displacement, could add a factor of about 5. Taking these factors into consideration gives a Rabi frequency in the range of 10–100 kHz. This Rabi frequency is still, in comparison to the charge-based quantum dot and SSET systems, a weak coupling and is vulnerable to dephasing from nuclear hyperfine fields. However, the future evolution of this technology may make such an approach feasible and desirable, especially considering the possible benefits of combining spintronics and nanomechanics.

VII. CONCLUSIONS

We have illustrated how quantum-coherent behavior and the energy spectrum of a nanomechanical resonator can be identified using full-frequency current-noise measurements through a nearby transport qubit. In the zero-frequency limit, we showed that a single-mode "environment," as represented by a nanomechanical resonator, produces unique signatures that differ from those observed in multimode environments. Furthermore, we identified regimes where phonon squeezing and cross-correlated noise, indications of complex quantum phenomena, could occur. All of these features could be realized with a double quantum dot or superconducting single-electron transistor operating as the transport qubit. In a broader context, we expect that noise measurements could also be useful in two-resonator circuit-QED systems,[25,42,43] which may offer an interesting area for future investigation.

ACKNOWLEDGMENTS

We thank Sahel Ashab, Christoph Bruder, Tobias Brandes, and Yueh-nan Chen for helpful discussions. F.N. acknowledges partial support from the National Security Agency (NSA), Laboratory for Physical Sciences (LPS), (U.S.) Army Research Office (ARO), and National Science Foundation (NSF) under Grant No. EIA-0130383.

APPENDIX: NOISE FORMALISM

To calculate the quantum noise[20] of a system with Hamiltonian H and corresponding transport environment described by a Liouvillian L, we employ a generating-function approach. The master equation for the matrix elements of the generating function $\mathbf{g}$ is

$$\frac{\partial}{\partial t}\mathbf{g}(s_1, \ldots, s_m, t) = M(s_1, \ldots, s_m)\mathbf{g}(s_1, \ldots, s_m, t), \quad (A1)$$

which can be formally solved by diagonalizing

$$M(s_1, \ldots, s_m) = V(s_1, \ldots, s_m)D(s_1, \ldots, s_m)V^{-1}(s_1, \ldots, s_m). \quad (A2)$$

Here M is the Liouvillian L recast as a function of the counting variables $(s_1, \ldots, s_m)$. Each s_i is a continuous variable which tracks the passage of the current through system i. This gives a general formalism for calculating the generating function of m coherent and interacting transport systems, each with a single "one-way" current flow.

The next step is to use the MacDonald formula[44] for the *symmetrized noise power correlator* between systems i and j,

$$S(\omega)_{i,j} \equiv \int_{-\infty}^{\infty} d\tau e^{i\omega\tau}[\langle \delta I_i(t+\tau), \delta I_j(t)\rangle]_{t\to\infty},$$

$$\frac{S(\omega)_{i,j}}{2e^2\omega} = \int_0^{\infty} \sin(\omega\tau)\partial_\tau\left(\langle n_i(\tau)n_j(\tau)\rangle - \frac{\tau^2\langle I_i\rangle\langle I_j\rangle}{e^2}\right), \quad (A3)$$

which can be written as $(s = \{s_1, s_2, \ldots, s_m\})$,

$$\frac{S(\omega)_{i,j}}{2e^2\omega} = (\partial_{s_i,s_j} + \delta_{i,j}\partial_{s_i})\int_0^\infty d\tau \sin(\omega\tau)\frac{\partial}{\partial\tau}\mathrm{Tr}\,\hat{G}(s\tau)|_{s=1}, \tag{A4}$$

where an omitted term $2\tau\langle I\rangle^2$ in the integral does not contribute in the final result obtained upon performing the Laplace transformation. Noting that $\hat{G}(s,\tau=0)=\rho(0)$, where the initial condition $\rho(0)$ is the steady-state-density matrix and using

$$\frac{\partial}{\partial\tau}\hat{G}(s,\tau) = M(s)\hat{G}(s,\tau) = M(s)e^{\tau M(s)}\hat{G}(s,\tau=0),$$

and the spectral decomposition of $M(s)$, one obtains

$$S(\omega)_{i,j} = 2e^2(\partial_{s_i,s_j} + \delta_{i,j}\partial_{s_i}) \times \left\| V(s)\frac{\omega^2 D(s)}{\omega^2 + D(s)^2}V^{-1}(s)\mathbf{g}(s,0)\right\|_{s=1}, \tag{A5}$$

where the notation $\|(x_{i_1,j_1},x_{i_2,j_2},\ldots,)\| \equiv \Sigma_{i=0}x_{ii}$ takes into account the trace in Eq. (A4). Note that the first derivative in the single system correlator ∂_s yields $2e\langle I\rangle$, and therefore ∂_s^2 provides the deviation from the shot noise. Using the Ramo-Shockley theorem,[20] the displacement-current contribution can either be omitted (by assuming that the capacitances of the devices are extremely asymmetric, so that $c_L c_R \ll 1$) or calculated using a multivariable approach because the total current fluctuations can be written as

$$\delta I(t+\tau)\delta I(t) = \alpha^2\delta I_L(t+\tau)\delta I_L(t+\tau) + \beta^2\delta I_R(t+\tau)\delta I_R(t) + \alpha\beta[\delta I_L(t+\tau)\delta I_R(t) + \delta I_R(t+\tau)\delta I_L(t)]. \tag{A6}$$

The left and right correlations are trivially calculated using separate counting variables for each lead.

Equation (A5) allows one to calculate the noise spectrum for transport through an arbitrarily complex quantum system. This can be evaluated either using finite difference derivatives around $s=1$ or following the methods employed by Flindt *et al.*[45,46] In the latter case we can use their approach to show that, in general, the cross correlator can be written as

$$\partial_t\langle n_i(t)n_j(t)\rangle = \mathrm{Tr}\left[L_i\sum_{n_1,n_2,\ldots} n_j\rho^{(n_1),(n_2),\ldots}\right] + \mathrm{Tr}\left[L_j\sum_{n_1,n_2,\ldots} n_i\rho^{(n_1),(n_2),\ldots}\right]. \tag{A7}$$

Furthermore the terms

$$\sum_{n_1,n_2,\ldots} n_j\rho^{(n_1),(n_2),\ldots} = \partial_{s_j}\hat{G}(s,\tau)|_{s=1} \tag{A8}$$

can be evaluated by Laplace transforming the equation of motion

$$\partial_\tau\hat{G}(s,t) = \left(L_0 + \sum_i s_i L_i\right)\hat{G}(s,t) \tag{A9}$$

and taking derivatives in the counting variables s_i, giving

$$\partial_{s_i}\tilde{G}(s,-i\omega)|_{s=1} = F(-i\omega)L_iF(-i\omega)\rho(0), \tag{A10}$$

where

$$F(-i\omega) = (-i\omega - L)^{-1} \tag{A11}$$

and $\rho(0)$ is the steady-state initial condition. As shown by Flindt *et al.*[45] one can evaluate this inverse by writing

$$F(-i\omega) = -P/i\omega - R(\omega), \tag{A12}$$

$$R(\omega) = Q(i\omega + L)^{-1}Q, \tag{A13}$$

where

$$P = \rho(0)\otimes 1, \quad Q = 1 - P. \tag{A14}$$

Inserting all these expressions into the cross correlator and using $P\rho(0)=\rho(0)$ and $Q\rho(0)=0$ give the noise power as the trace of an inverse,

$$\frac{S(\omega)_{i,j}}{2e^2} = \mathrm{Re}\{-\mathrm{Tr}[L_iR(\omega)L_j\rho(0)] - \mathrm{Tr}[L_jR(\omega)L_i\rho(0)]\} + \delta_{i,j}\,\mathrm{Tr}[L_i\rho(0)]. \tag{A15}$$

All of the above allows us to calculate the full-frequency spectrum for an arbitrary number of coupled systems. In addition, it allows us to calculate *phonon* current and statistics. We choose as the phonon current operator the operator which absorbs a phonon number state from the mode and sets it in the background bath.

*nwlambert@riken.jp

[1] H. G. Craighead, Science **290**, 1532 (2000).
[2] A. Cho, Science **299**, 36 (2003).
[3] K. Schwab and M. Roukes, Phys. Today **58**(7), 36 (2005).
[4] P. Treutlein, D. Hunger, S. Camerer, T. W. Hansch, and J. Reichel, Phys. Rev. Lett. **99**, 140403 (2007).
[5] L. F. Wei, Y. X. Liu, C. P. Sun, and F. Nori, Phys. Rev. Lett. **97**, 237201 (2006).
[6] M. Blencowe, Contemp. Phys. **46**, 249 (2005).
[7] N. Lambert, I. Mahboob, M. Pioro-Ladriere, Y. Tokura, S. Tarucha, and H. Yamaguchi, Phys. Rev. Lett. **100**, 136802 (2008).
[8] D. A. Rodrigues, J. Imbers, and A. D. Armour, Phys. Rev. Lett. **98**, 067204 (2007).
[9] A. Naik, O. Buu, M. D. LaHaye, A. D. Armour, A. A. Clerk, M. P. Blencowe, and K. C. Schwab, Nature (London) **443**, 193 (2006).
[10] S.-H. Ouyang, J. Q. You, and F. Nori, arXiv:0807.4833 (unpublished).
[11] E. M. Weig, R. H. Blick, T. Brandes, J. Kirschbaum, W. Wegscheider, M. Bichler, and J. P. Kotthaus, Phys. Rev. Lett. **92**, 046804 (2004).

[12] G. Kieszlich, E. Schöll, T. Brandes, F. Hohls, and R. J. Haug, Phys. Rev. Lett. **99**, 206602 (2007).
[13] N. Lambert, R. Aguado, and T. Brandes, Phys. Rev. B **75**, 045340 (2007).
[14] C. W. J. Beenakker, C. Emary, M. Kindermann, and J. L. van Velsen, Phys. Rev. Lett. **91**, 147901 (2003).
[15] T. Brandes and N. Lambert, Phys. Rev. B **67**, 125323 (2003).
[16] S. D. Bennett and A. A. Clerk, Phys. Rev. B **74**, 201301(R) (2006).
[17] F. Xue, Y. X. Liu, C. P. Sun, and F. Nori, Phys. Rev. B **76**, 064305 (2007).
[18] T. Brandes, Phys. Rep. **408**, 315 (2005).
[19] R. Aguado and T. Brandes, Phys. Rev. Lett. **92**, 206601 (2004).
[20] Y. M. Blanter and M. Buttiker, Phys. Rep. **336**, 1 (2000).
[21] F. Deppe, M. Mariantoni, E. P. Menzel, A. Marx, S. Saito, K. Kakuyanagi, H. Tanaka, T. Meno, K. Semba, H. Takayanagi, E. Solano, and R. Gross, Nat. Phys. **4**, 686 (2008).
[22] J. Q. You and F. Nori, Phys. Today **58**(11), 42 (2005).
[23] J. Q. You and F. Nori, Physica E (Amsterdam) **18**, 33 (2003).
[24] J. Q. You and F. Nori, Phys. Rev. B **68**, 064509 (2003b).
[25] M. Mariantoni, M. J. Storcz, F. K. Wilhelm, W. D. Oliver, A. Emmert, A. Marx, R. Gross, H. Christ, and E. Solano, arXiv:cond-mat/0509737 (unpublished).
[26] C. Emary, D. Marcos, R. Aguado, and T. Brandes, Phys. Rev. B **76**, 161404(R) (2007).
[27] C. Flindt, T. Novotny, A. Braggio, M. Sassetti, and A.-P. Jauho, Phys. Rev. Lett. **100**, 150601 (2008).
[28] M. Hofheinz, E. M. Weig, M. Ansmann, R. C. Bialczak, E. Lucero, M. Neeley, A. D. O'Connell, H. Wang, J. M. Martinis, and A. N. Cleland, Nature (London) **454**, 310 (2008).
[29] J. M. Fink, M. Göppl, M. Baur, R. Bianchetti, P. J. Leek, A. Blais, and A. Wallraff, Nature (London) **454**, 315 (2008).
[30] I. Schuster, A. Kubanek, A. Fuhrmanek, T. Puppe, P. W. H. Pinkse, K. Murr, and G. Rempe, Nat. Phys. **4**, 382 (2008).
[31] A. N. Omelyanchouk, S. N. Shevchenko, A. M. Zagoskin, E. Il'ichev, and F. Nori, Phys. Rev. B **78**, 054512 (2008).
[32] S. Shevchenko, A. Omelyanchouk, A. Zagoskin, S. Savel'ev, and F. Nori, New J. Phys. **10**, 073026 (2008).
[33] M. Grajcar, S. Ashhab, J. R. Johansson, and F. Nori, Phys. Rev. B **78**, 035406 (2008).
[34] X. Hu and F. Nori, Phys. Rev. B **53**, 2419 (1996).
[35] X. Hu and F. Nori, Phys. Rev. Lett. **76**, 2294 (1996).
[36] X. Hu and F. Nori, Phys. Rev. Lett. **79**, 4605 (1997).
[37] X. Hu and F. Nori, Physica B **263–264**, 16 (1999).
[38] M. C. Teich and B. E. A. Saleh, *Progress in Optics* (Elsevier Science, Amsterdam, 1988), Vol. 26.
[39] L. Mandel and E. Wolf, *Optical Coherence and Quantum Optics* (Cambridge University Press, Cambridge, 1995).
[40] M. A. Castellanos-Beltran, K. D. Irwin, G. C. Hilton, L. R. Vale, and K. W. Lehnert, Nat. Phys. (unpublished).
[41] T. J. Harvey, D. A. Rodrigues, and A. D. Armour, Phys. Rev. B **78**, 024513 (2008).
[42] C. P. Sun, L. F. Wei, Y. X. Liu, and F. Nori, Phys. Rev. A **73**, 022318 (2006).
[43] C. A. Regal, J. D. Teufel, and K. W. Lehnert, Nat. Phys. **4**, 555 (2008).
[44] D. K. C. MacDonald, *Noise and Fluctuations* (Wiley, New York, 1962).
[45] C. Flindt, T. Novotny, and A.-P. Jauho, Phys. Rev. B **70**, 205334 (2004).
[46] C. Flindt, T. Novotny, and A.-P. Jauho, Europhys. Lett. **69**, 475 (2005).